



## Research Article

# Boosting the Stability at Room Atmosphere of Lead Halide Perovskites Through a Simultaneous Compositional Tuning of the A-and X-sites

Sié Georges Hien<sup>1,2\*</sup> , Amal Bouich<sup>1</sup> , Abou Bakary Coulibaly<sup>2</sup> , Aka Boko<sup>2</sup>, Bernabé Marí Soucase<sup>1</sup> 

<sup>1</sup>Laboratory of New Materials for Photovoltaic Energy, Polytechnic University of Valencia, Spain

<sup>2</sup>Laboratory of Fundamental and Applied Sciences Research and Training Unit, University Nanguy Abrogoua, Côte d'Ivoire  
E-mail: Siehgb@yahoo.com

**Received:** 2 June 2023; **Revised:** 2 July 2023; **Accepted:** 10 July 2023

**Abstract:** Organic-inorganic lead halide perovskites, particularly the Formamidinium and Cesium based-ones are among the most promising materials for photovoltaic applications, yet they still face a stability issue. In this work, we boosted their structural and environment-resistance stability by the simultaneous compositional tuning of their A-cation and X-anion sites. We prepared 9 different solutions of  $\text{Cs}_x\text{FA}_{1-x}\text{Pb}(\text{I}_{1-y}\text{Br}_y)_3$  ( $x = 0.1, 0.2$  and  $0.3$  and  $y = 0.15, 0.25$  and  $0.35$ ), made the deposition on FTO substrates by one step spin-coating technique and did the post-annealing at  $120^\circ\text{C}$  instead of the  $350^\circ\text{C}$  for  $\text{CsPbI}_3$ , for instance. We, afterward, characterized the films by X-ray diffraction (XRD), UV-visible spectroscopy, photoluminescence (PL) levels and Field Emission Scanning Electron Microscopy (FESEM) to assess their crystallinity, optical properties and morphology. As a result, we noted that they all crystallized into the perovskite black  $\alpha$ -phase and remained stable after 3 weeks in contrast to  $\text{FAPbI}_3$  or  $\text{CsPbI}_3$ . We also found that their band gap energy ranged between  $1.62\text{ eV}$  (for the compounds with 15% of Br) to  $1.75\text{ eV}$ , hence their excellent absorbance properties.

**Keywords:** perovskite,  $\text{Cs}_x\text{FA}_{1-x}\text{Pb}(\text{I}_{1-y}\text{Br}_y)_3$ , band gap, stability,  $\alpha/\beta/\gamma/\delta$ -phase transition, solar cells, SCAPS, efficiency

## 1. Introduction

The recent decades have seen the blooming of the organic-inorganic metal halide perovskites in the photovoltaic material research arena. In a very short period, the perovskites have reached a high Power Conversion Efficiency (PCE) of 26% in 2023 [1, 2] which is already equivalent to the efficacy level of marketed silicon solar cells.

Despite the accomplishment in terms of PCE and their easy and low-cost production at ambient conditions, the perovskites still have steps to take to pass the International Electrotechnical Commission (IEC) 61215-1:2016 qualification requirements as terrestrial photovoltaic (PV) modules suitable for long-term operation in general open-air climates [3, 4] and exhibit a guaranteed operation ability of 25 years like the Silicon [5].

Actually, the commercialization of the perovskites is hindered by thermal, structural, moisture and light-related stability issues.

To overcome these bottlenecks, researchers have worked out better encapsulation technics like ionic-liquid additives and Lewis acid-base passivation, etc [6]. However, all these efforts have yielded limited results as the intrinsic

Copyright ©2023 Sié Georges Hien, et al.  
DOI: <https://doi.org/10.37256/aecm.4220233148>  
This is an open-access article distributed under a CC BY license  
(Creative Commons Attribution 4.0 International License)  
<https://creativecommons.org/licenses/by/4.0/>

instability has to be solved.

The Halide Perovskites have a generic  $ABX_3$  structure [7] where A is a monovalent cation such as Methylammonium ( $CH_3NH_3^+$ ; MA), Formamidinium ( $H_2NCHNH_2$ , FA) or Cesium (Cs); B is a divalent cation, typically Lead ( $Pb^{2+}$ ) or Tin ( $Sn^{2+}$ ) and X a halide anion such as Chloride (Cl), Bromide (Br) or Iodide (I). In this compound, it is proved that the A cation has the highest impact on the overall stability [8] of the lattice.

Among these A cations, researchers have demonstrated that the organic FA and the inorganic Cs have better stability compared to MA [9-10]. FA has a lower band gap at 1.48 eV (Cs has 1.73 eV), hence a higher potential to harvest more photons and Cs is more environment resistant. However, both show structural instability [11]. FA-based perovskites crystallize in the desired cubic crystal structure at high temperatures above 170 °C but at room temperatures, their structure shifts to the undesired yellow non-perovskite-phase crystal structure. Cs-based ones behave the same way from above 350 °C to room temperature [12]. In fact, Cs-based crystals can exist in four phases: the cubic phase ( $\alpha$ ), the tetragonal phase ( $\beta$ ), and two orthorhombic phases ( $\gamma$  and  $\delta$ ) [13]. The  $\delta$  orthorhombic, is the non-photoactive and non-perovskite 'yellow phase, useless in photovoltaic applications [14]. As for the  $\alpha$ ,  $\beta$  and  $\gamma$  phases, they exhibit 'black phase' perovskite structure but are only stable at high temperatures. Similarly, FA also exists in the same phases but at other temperatures and is also stable in the non-perovskite 'yellow phase' at room temperatures.

The B-cation in  $ABX_3$  is usually  $Pb^{2+}$  as researchers have evidenced an increase of instability and band gap when replacing the  $Pb^{2+}$  by  $Sn^{2+}$  [15-16].

As for the Anion X, I is the preferred one that exhibits a lower band gap while the others and much more Cl raise the band gap to undesired levels and lead to poor lattice parameters.

One of the usual approaches to improve the stability of the Halide Perovskites is the inclusion of additives. Tang et al. [17] for instance, were able to master the A-site composition by doping with some alkali metal cations such as Li, Na, K, and Rb to adjust the lattice constant and energy status.

In the same way, the B-site can be doped with lanthanide ions like  $La^{3+}$ ,  $Ce^{3+}$ ,  $Nd^{3+}$ ,  $Sm^{3+}$ ,  $Eu^{3+}$ ,  $Gd^{3+}$ ,  $Tb^{3+}$ ,  $Ho^{3+}$ ,  $Er^{3+}$ ,  $Yb^{3+}$ , and  $Lu^{3+}$  or hard Lewis acids such as  $Mg^{2+}$ ,  $Ca^{2+}$ ,  $Sr^{2+}$ , and  $Ba^{2+}$  [18].

Another way of stability enhancement is the composition of lower dimensional entities, such as nanocrystals (NCs), materials with dimensions smaller than their corresponding Bohr exciton radius, named quantum dots [19]. These materials exhibit the quantum confinement effect that induces their unique physical characteristics like a size-tunable bandgap, narrow emission spectra, a high surface/volume ratio, key factors to reach an improved crystalline phase stability at ambient conditions, compared to their bulk equivalents. This method requires, however, specific equipment and demanding processing.

In this work, we rather focused on the compositional tuning of the A and X-sites in the room atmosphere to improve the stability of the  $ABX_3$  compound [20]. We brought together the two FA and Cs cations in the A-cation and the I and Br anions in the X-cation. We found this method easier and cheaper than the above ones whilst efficient. The challenge, however, has been the increase in band gap as this is the known tendency when Br anion is incorporated into the lattice.

In a former study on the  $Cs_xFA_{1-x}PbI_3$  structure, we've seen that mixing the two A-cations Cs and FA leads to a more stable lattice when the proportion of Cs is less than FA, preferably not more than 30% [21]. Therefore, in our present investigation, we mixed [22] the cations A and X in the same thin film lattices through a structure type  $Cs_xFA_{1-x}Pb(I_{1-y}Br_y)_3$  and varied, simultaneously, the content of Cs in the lattice from 10% to 30% for percentages of Br from 15% to 35%. The goal that guided our investigation was to figure out which of the samples exhibit the perovskite  $\alpha$ -phase after being manufactured at room temperature and if they would remain stable for long in that phase [23].

Furthermore, we closely looked at the annealing temperature while composing our material and selecting our solvents. Since the shift temperature of Cs and FA-based compounds from the non-perovskite phase to the cubic perovskite phase takes place at high temperatures [24-25], their synthesis induces a thermal annealing treatment at elevated temperatures. This situation does inflate the production cost of the halide perovskites and can also prevent their deposition on polymer-based flexible substrates, hence the need to reduce the annealing temperature of our films.

After the synthesis, the different characterization methods helped us cross-check the stability of each sample along with the identification of the best compound. In the next pages of this article, the samples were identified by their report names in Table 1. In the CB-xyyy format, C stands for Cesium, B for Bromide, xx (10, 20 or 30) is the Cesium content in the  $Cs_xFA_{1-x}Pb(I_{1-y}Br_y)_3$  compound and yy (15, 25 or 35) the bromide content.

## 2. Experimental work

With the combination of three contents of the A-cation Cs with three of Br Anion, we reached a total of nine (9) samples to be produced by first synthesizing the solutions and then making the deposition on FTO substrates.

**Table 1.** List of samples blended and characterized

Cs Content	Br Content	$\text{Cs}_x\text{FA}_{1-x}\text{Pb}(\text{I}_{1-y}\text{Br}_y)_3$ Composition	Report Name
0.1	0.15	$\text{Cs}_{0.1}\text{FA}_{0.9}\text{Pb}(\text{I}_{0.85}\text{Br}_{0.15})_3$	CB-1015
0.1	0.25	$\text{Cs}_{0.1}\text{FA}_{0.9}\text{Pb}(\text{I}_{0.75}\text{Br}_{0.25})_3$	CB-1025
0.1	0.35	$\text{Cs}_{0.1}\text{FA}_{0.9}\text{Pb}(\text{I}_{0.65}\text{Br}_{0.35})_3$	CB-1035
0.2	0.15	$\text{Cs}_{0.2}\text{FA}_{0.8}\text{Pb}(\text{I}_{0.85}\text{Br}_{0.15})_3$	CB-2015
0.2	0.25	$\text{Cs}_{0.2}\text{FA}_{0.8}\text{Pb}(\text{I}_{0.75}\text{Br}_{0.25})_3$	CB-2025
0.2	0.35	$\text{Cs}_{0.2}\text{FA}_{0.8}\text{Pb}(\text{I}_{0.65}\text{Br}_{0.35})_3$	CB-2035
0.3	0.15	$\text{Cs}_{0.3}\text{FA}_{0.7}\text{Pb}(\text{I}_{0.85}\text{Br}_{0.15})_3$	CB-3015
0.3	0.25	$\text{Cs}_{0.3}\text{FA}_{0.7}\text{Pb}(\text{I}_{0.75}\text{Br}_{0.25})_3$	CB-3025
0.3	0.35	$\text{Cs}_{0.3}\text{FA}_{0.7}\text{Pb}(\text{I}_{0.65}\text{Br}_{0.35})_3$	CB-3035

### 2.1 Solutions synthesis

For the preparation of the solutions, we used four (4) precursors which were the Formamidinium Iodide (FAI), the Cesium Iodide (CsI), the Lead Iodide ( $\text{PbI}_2$ ) and the Lead Bromide ( $\text{PbBr}_2$ ).

The solvent was a mixture (Cosolvent) of DMF (Dimethyl Formamide- $\text{HCON}(\text{CH}_3)_2$ ) and DMSO (Dimethyl Sulfoxide) in a ratio of 4:1. As for the anti-solvent, we used the Toluene ( $\text{C}_6\text{H}_5\text{CH}_3$ ).

The CsI,  $\text{PbBr}_2$  and  $\text{PbI}_2$  were purchased from Tokyo Chemical Industry and the FAI from Sigma-Aldrich. As for the DMF, DMSO and Toluene, the sellers were respectively VWR International France and Applichem GmbH, Germany.

After the calculation of the compositions of each material for a concentration of 1 M per liter for all solutions, the precursors have been weighed out and put in the same vial before adding one (1) mL of cosolvent to dissolve them.

### 2.2 Deposition method

The deposition as illustrated in Figure 1 was then done by one-step spin-coating on FTO substrates while applying Toluene anti-solvent to evaporate the solvent. A post-annealing was done at 120 °C for 30 min to obtain the black perovskite films.

The spin-coated films were then characterized by X-Ray Diffraction (XRD) [26], UV-visible spectroscopy, Photoluminescence (PL) measurements and Field Emission Scanning Electron Microscopy (FESEM) to capture their crystallinity, optical properties, and morphology.

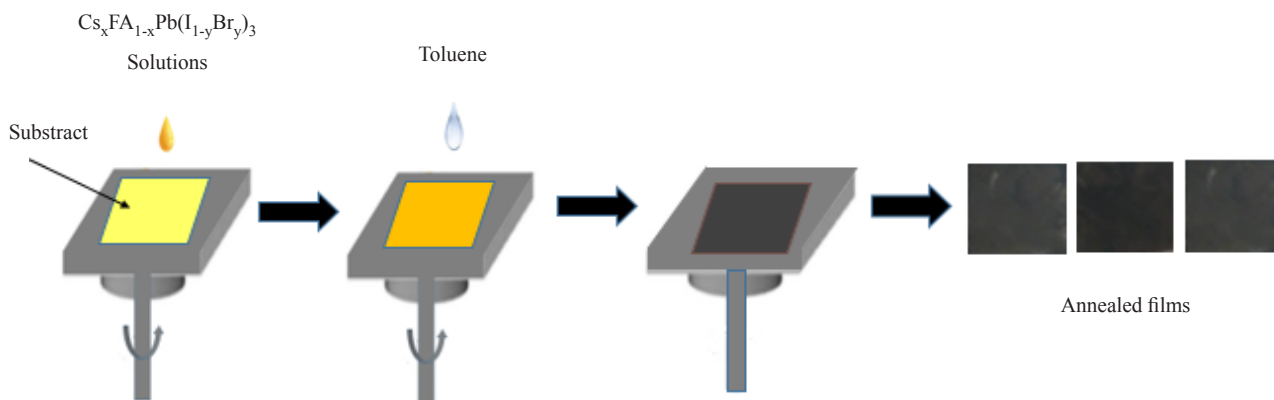


Figure 1. One-step films Spin-coating

### 3. Results and discussion

#### 3.1 Structure analysis

The X-Ray diffraction patterns of the perovskite samples on FTO substrates were generated by a RIGAKU Ultima IV using a  $\text{Cu K}\alpha$  radiation ( $\lambda = 1.541841 \pm 0.002 \text{ \AA}$ ). This characterization is technic enables to identification of the crystal phase and the crystallinity of the material. It allows as well to visualize the forming of the perovskite as well as its degradation.

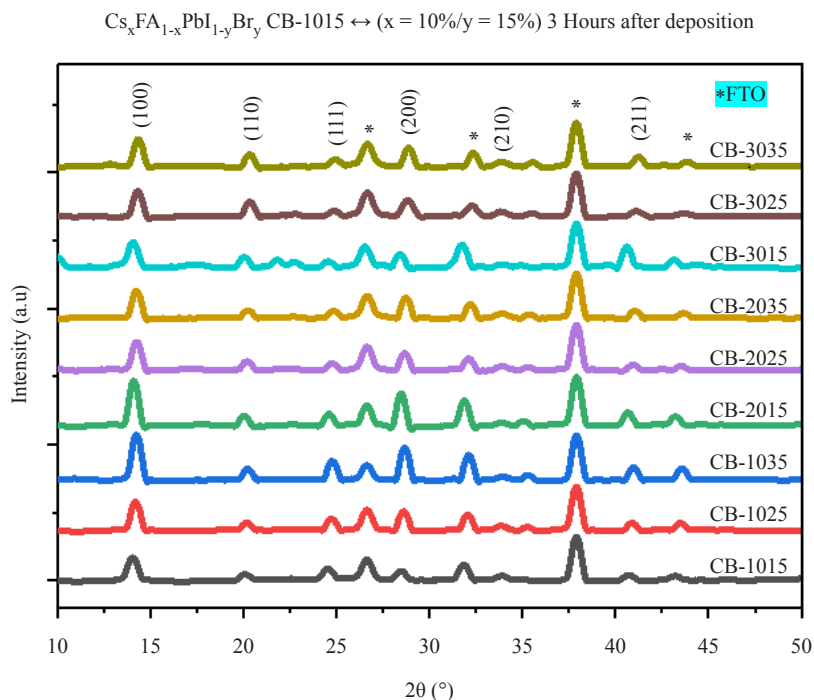
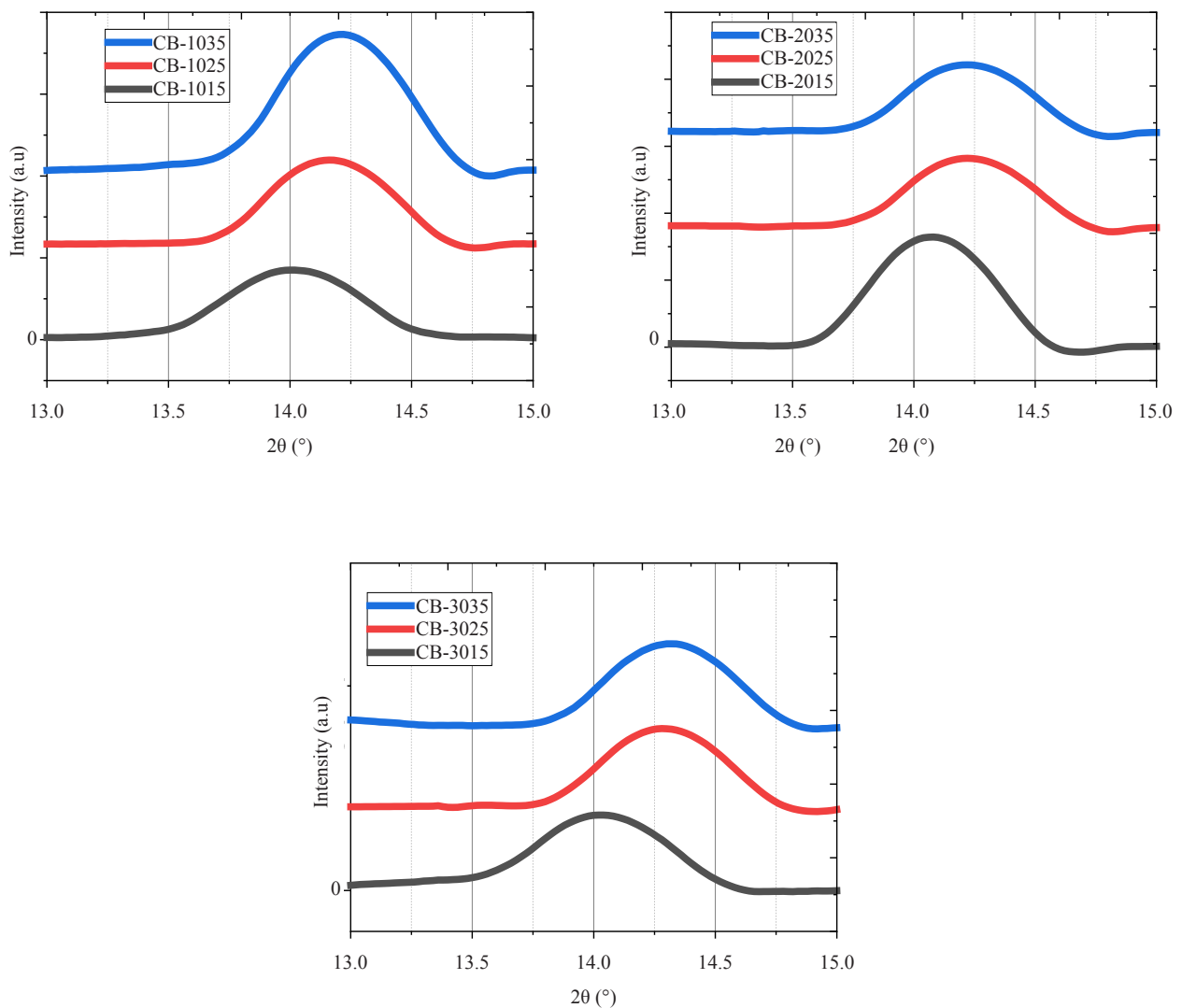


Figure 2. XRD patterns of  $\text{Cs}_x\text{FA}_{1-x}\text{Pb}(\text{I}_{1-y}\text{Br}_y)_3$  samples deposited on FTO Substrate

Figure 2 exhibits the XRD patterns of the nine (9)  $\text{Cs}_x\text{FA}_{1-x}\text{Pb}(\text{I}_{1-y}\text{Br}_y)_3$  ( $x = 10\%, 20\%, 30\%, y=15\%, 25\%, 35\%$ ) films blended at room temperature.

The characteristic peaks [27] (100), (110), (111), and (200) reflection plans of the perovskite  $\alpha$ -phase were clearly visible at  $2\theta$  values around  $14^\circ$ ,  $20^\circ$ ,  $24.5^\circ$  and  $28.3^\circ$  respectively, for all the films. This showed that, in contrast to  $\text{CsPbI}_3$  or  $\text{FAPbI}_3$  films, the mixed  $\text{Cs}_x\text{FA}_{1-x}\text{Pb}(\text{I}_{1-y}\text{Br}_y)_3$  perovskites crystallized in the  $\alpha$ -phase at room temperature. We've also noted a clear black color of all the films as further evidence of the formation of the perovskite  $\alpha$ -phase.

We also noted, as illustrated by Figure 3, that the peak position ( $2\theta$ ) shifted towards the right, to higher values as per the increase of the Br content ( $y$ ) in the lattice, which implied a larger band gap for the material. The Cs content ( $x$ ) also had a similar impact but in a smaller proportion.



**Figure 3.** Effect of Br content ( $y$ ) on the position ( $2\theta$ ) of the peaks of  $\text{Cs}_x\text{FA}_{1-x}\text{Pb}(\text{I}_{1-y}\text{Br}_y)_3$  samples

We further calculated the crystallite size  $D$ , the lattice dislocation and Lattice strain out of the FWHM (maximum width at half maximum) and  $2\theta$  of peak positions using the Scherrer Equation and other related relations. The results are illustrated in Figure 4. These values inform about the quality of the microscopic structure inside the lattice.

Crystallite is a domain of the material with a homogeneous arrangement of the atoms or molecules that repeat itself

to form the grains and then the particles. In terms of diffraction, the crystallite is a portion of the crystal that diffracts light coherently (in the same direction), the crystallite size being the dimension of that homogeneous area.

The crystal structures usually present defects or dislocations that induce sudden shifts in the arrangement of the atoms and this generates the observable broadening of the diffraction peaks. The dislocation density is the measure of the number of dislocations in a unit volume.

As for the lattice strain, it is a quantification of the distribution of lattice constraints arising from crystal imperfections, such as lattice dislocation. The crystallite size and lattice strain affect the peak width, peak intensity and  $2\theta$  angle peak position.

The crystallite size was calculated by the formula [28]:

$$D = \frac{kx\lambda}{\beta x \cos \theta}$$

k: Scherrer's Constant = 0.94.

$\lambda$ : X-ray wavelength = 1.5406 Å.

$\beta$ : FWHM of the diffraction peak.

$\theta$ : Angle of diffraction.

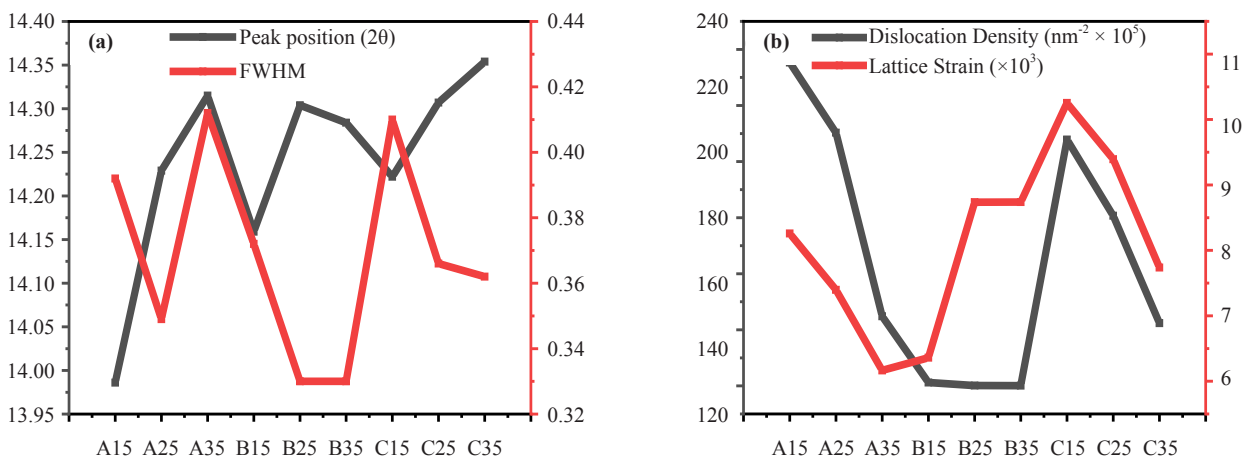
The dislocation density,  $\delta$ , defined as the length of dislocation lines per unit volume is calculated by:

$$\delta = \frac{1}{D^2}$$

As for the Lattice strain, its formula is:

$$\epsilon = \frac{\beta}{4x \tan \theta}$$

The calculations were done for each peak of the materials (peaks of FTO exclusive) and the average taken. Figure 4 represents a summary of the results.



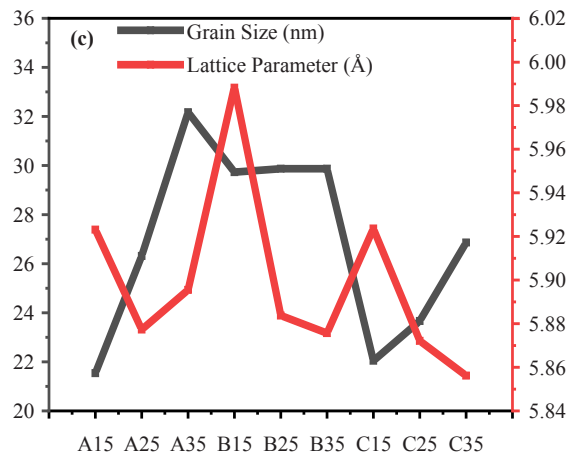
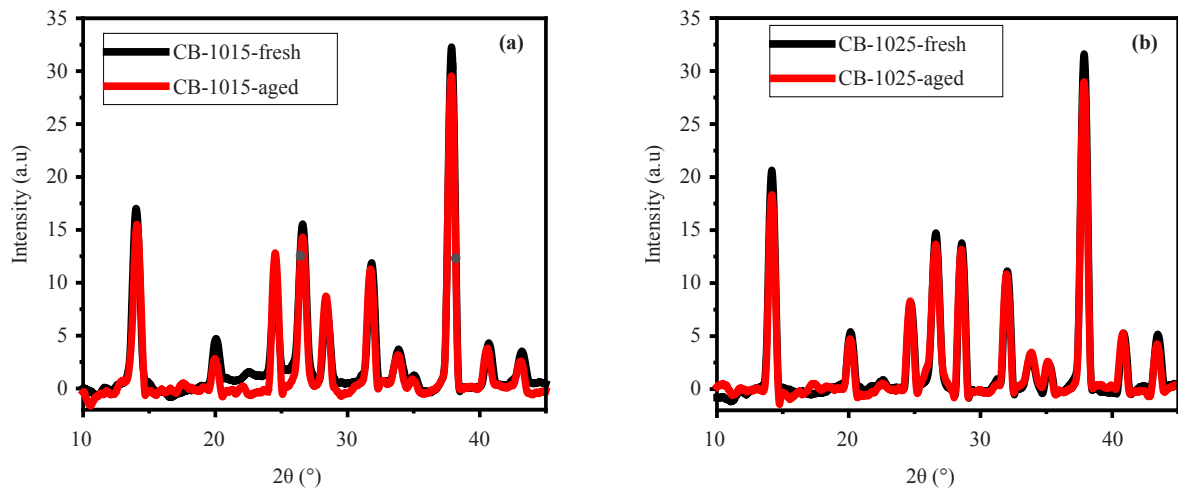


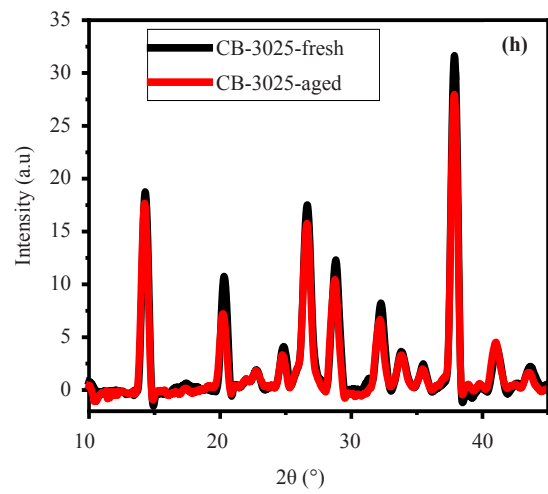
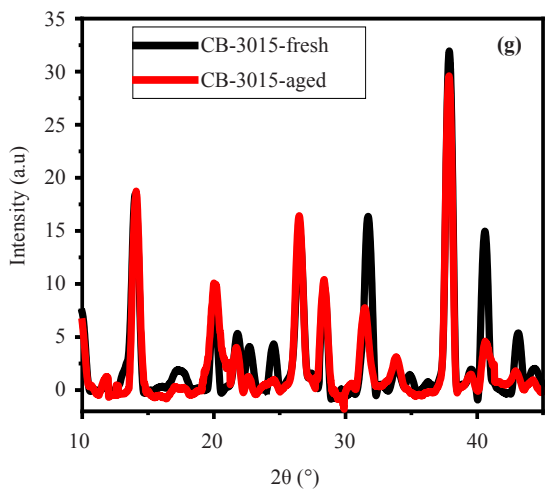
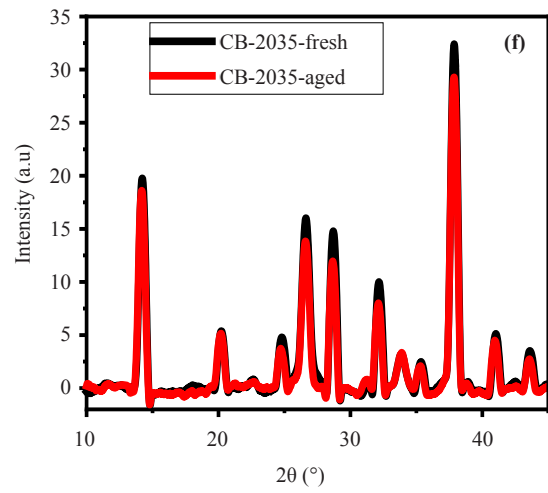
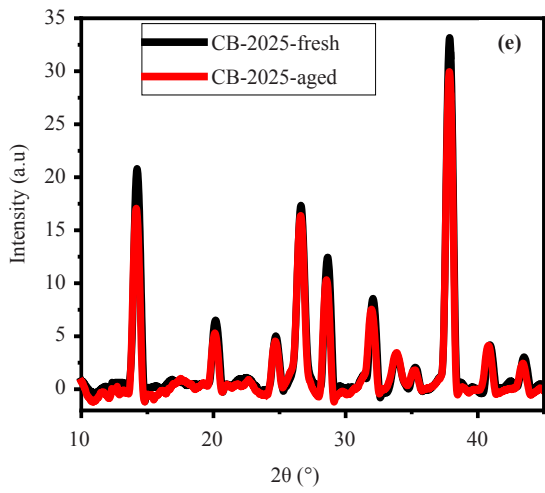
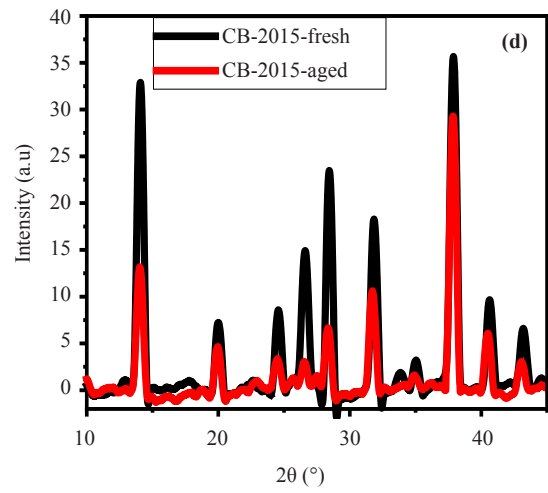
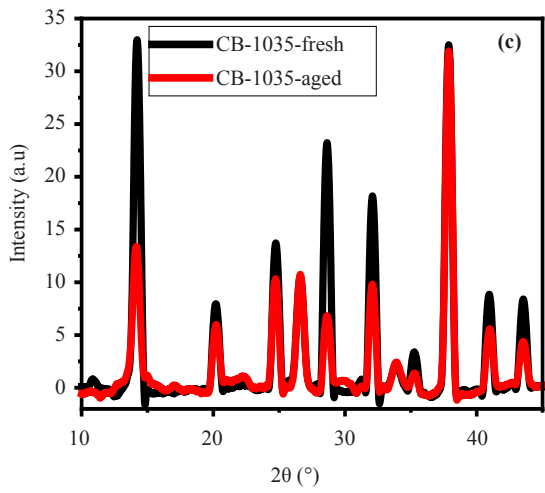
**Figure 4.** a) Peak position and FWHM, b) Dislocation and Lattice Strain, and c) Grain size and Lattice constant. (A15-A35 stands respectively for CB-1015-CB-1035, B15-B35 for CB-2015-CB-2035 and C15-C35 for CB-3015-CB-3035)

We noted that the diffraction peaks exhibited different tendencies according to the composition of the perovskite materials as some are broader and others thick even with the same content of Cs for instance. We further observed that for the same Cs content (10%, 20% or 30%), the compounds with less Br showed smaller grain size. This appears to be in line with the fact that Bromine's atom has a smaller diameter compared to Iodine. On the other hand and except for the CB-1035, the peaks of these low Br samples were thicker than the average, hence their higher crystallite size. This implies that the lattice with more bromine exhibits more imperfections. As for the lattice constant and as expected, it globally decreased with increasing crystallite size while the lattice strain raised with more crystallite size.

Three weeks after the first XRD analysis, we did a new checking with the Rigaku equipment.

Figure 5 gives the new patterns in red superimposed on the former ones for the sake of comparison.





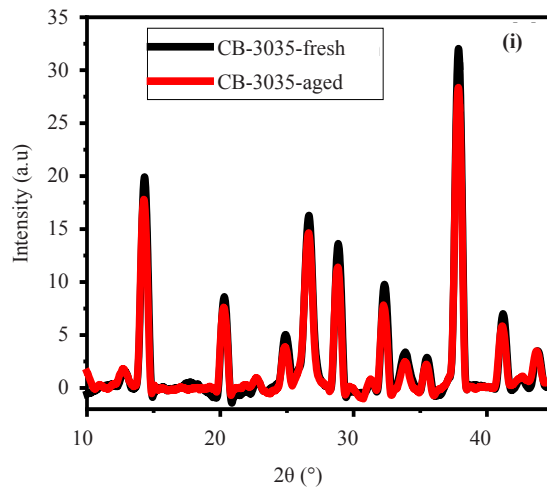


**Figure 5.** XRD patterns of  $\text{Cs}_x\text{FA}_{1-x}\text{Pb}(\text{I}_{1-y}\text{Br}_y)_3$  samples after 3 weeks

During the three weeks, the samples were conserved in the laboratory at room conditions without a particular protection.

We observed, except with the samples CB-1035 (c) and CB-2015(d), that most of the samples clearly demonstrated excellent structural and environmental-resistance stability as only a slight decrease in the intensity of the peaks was seen. Furthermore, we noticed that the angles of diffraction ( $2\theta$ ) of the peaks remained the same, meaning that the lattice structures had been preserved.

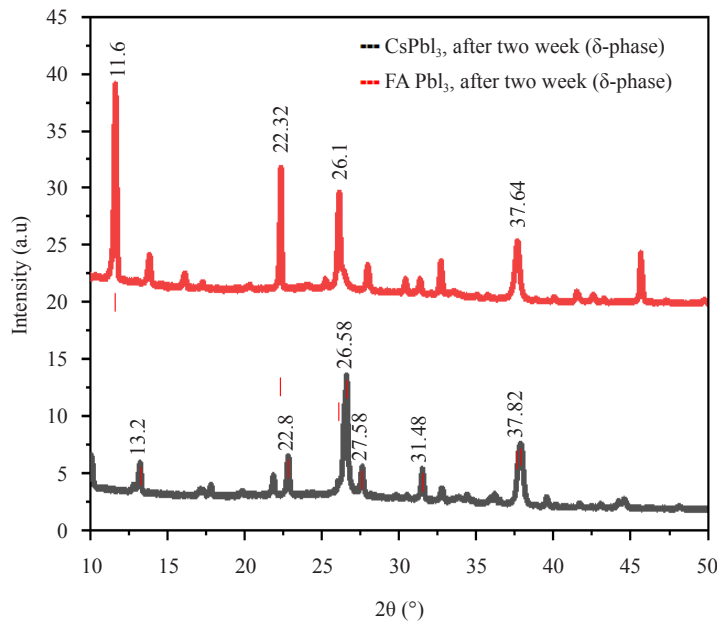


**Figure 6.** XRD patterns of  $\text{CsPbI}_3$  and  $\text{FAPbI}_3$  samples after 3 weeks

Two films among the nine, CB-1035 and CB-2015, exhibited the highest degradation and we suspect a problem

during the post-annealing (the samples may have not been exposed to enough heat) and/or their contamination during the conservation at the laboratory as the reason for this larger degradation revealed by the XRD testing.

Overall, we can say that three weeks after, at room conditions, the  $\text{Cs}_x\text{FA}_{1-x}\text{Pb}(\text{I}_{1-y}\text{Br}_y)_3$  perovskite structures, clearly exhibited a much better stability in the  $\alpha$ -phase than the single A-cation-based compounds like  $\text{FAPbI}_3$  or  $\text{CsPbI}_3$  for instance (Figure 6) which prompt to structurally degrade into a non-perovskite  $\delta$ -phase at room temperature.

We note that the two samples have shifted to the non-perovskite  $\delta$ -phase with the characteristic peaks at 13.2 and 11.6 instead of 14.

### 3.2 Optical properties assessment

The optical properties were collected with a spectrometer Ocean Optics HR4,000 connected to a Si-CCD detector and a combined sphere to capture luminance and diffuse transmittance at room conditions. As for the photoluminescence (PL) checking, we used a back-thinned Si-CCD Hamamatsu sensor with a He-Cd laser at 405 nm as an emission source.

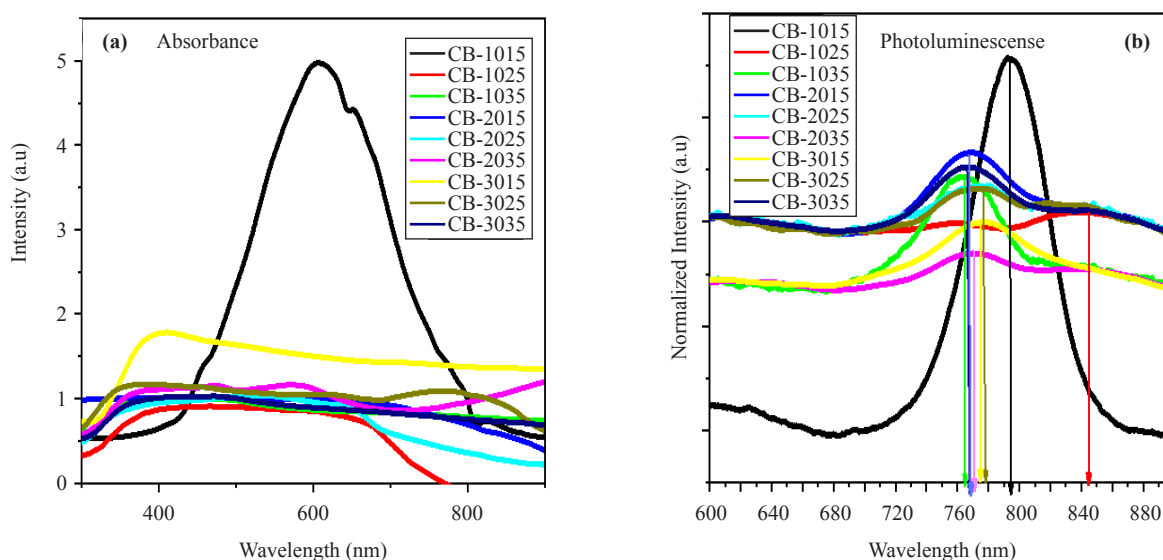
The absorbance properties are particularly important as the aim of the solar cell is to absorb the solar light and convert it into electricity. Besides, they can be used to calculate the band gap energy of the samples using the Tauc equation  $((\alpha h\nu)^2 = A(h\nu - E_g))$  [29-30]. The band gap is the value of  $E_g$  for which the  $(\alpha h\nu)^2 = 0$  after plotting the graph of  $(\alpha h\nu)^2$  versus  $h\nu$ .

In the Tauc formula,  $\alpha$  is the absorption coefficient,  $h$  the Planck's constant equal to  $6.625 \times 10^{-34}$  j.s,  $\nu$  the incident photon's frequency,  $A$  a proportionality constant and  $E_g$  is the bang gap energy.

On the other hand, the photoluminescence data can also be used to calculate a direct band gap using the formula  $E = hc/\lambda$  [31-32].

Figure 7 shows the absorbance, photoluminescence and band gap calculation of the samples.

We noted that most of the absorbance curves exhibited a tipping point at around 300 nm (500 nm for the CB-1015 as the exception) from which started an intense upward slope of absorbance corresponding to the excitonic absorbance [33-34], followed by a more or less stable phase, the crossing phase from the valence band to the conduction band. In the situation where this phase prevails over the others in the absorbance spectrum, the well-known Tauc formula linking the absorption coefficient ( $\alpha$ ) and the bandgap energy ( $E_g$ ), and widely used to calculate the direct band gap of semiconductors no more works. It is rather Elliott's formula that has to be used [35].



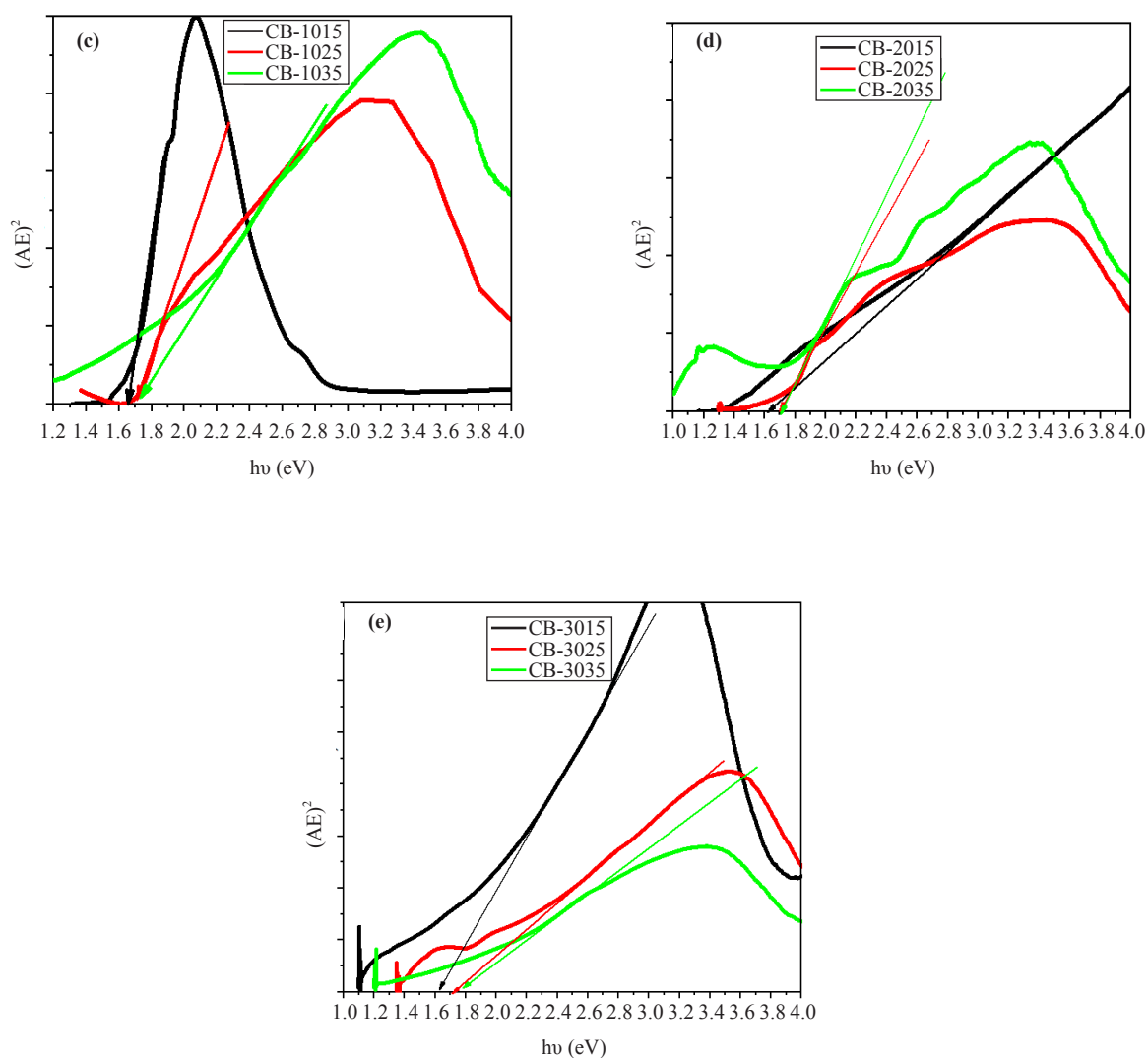


**Figure 7.** UV-vis Absorbance (a); Optical Band Gap from Absorbance (c, d, e) and Photoluminescence (b) of the  $\text{Cs}_x\text{FA}_{1-x}\text{Pb}(\text{I}_{1-y}\text{Br}_y)_3$  perovskite films

For the CB-1015 (10%-CS and 15%-Br), its absorbance curve exhibited an exceptional bell curve very similar to the sunlight absorption spectrum with the peak shifted to the right to 700 nm instead of 500 nm for the sunlight absorption spectra. This could be the result of a better surface coverage during the spin-coating associated with less degradation at the time of the absorbance measurement. The main challenge we usually face when measuring the absorbance properties of perovskite thin films is the lack of uniformity of the deposition on the substrate. With the bad coverage of the substrate, an important part of the light just unexpectedly goes through the blank areas uncovered by the perovskite material. In reverse, for the perovskite “mounts” where the material is concentrated, the optical density is most of the time very large and as a matter of fact, most of the light is absorbed. Consequently, the overall absorbance of the measured material can be altered [35].

The absorbance edge, as illustrated in Table 2 varied from the lowest value of 1.62 for the CB-xx15 (the three samples with 15% Br in the compound) to 1.75 for the CB-3035.

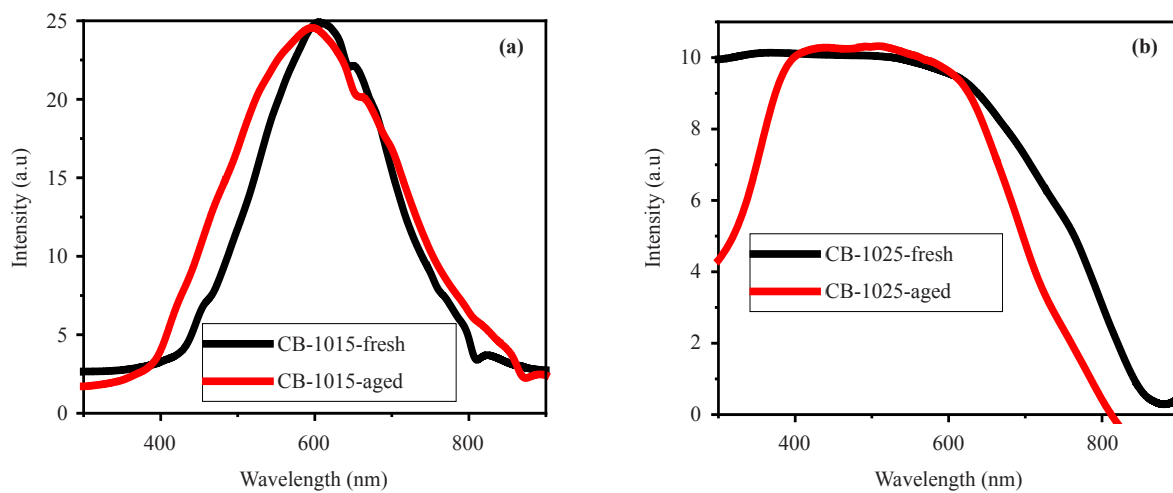
It increased with the content of the bromide halogen ion in the lattice and also with more or less the increase in the content of A-site Cesium cation.

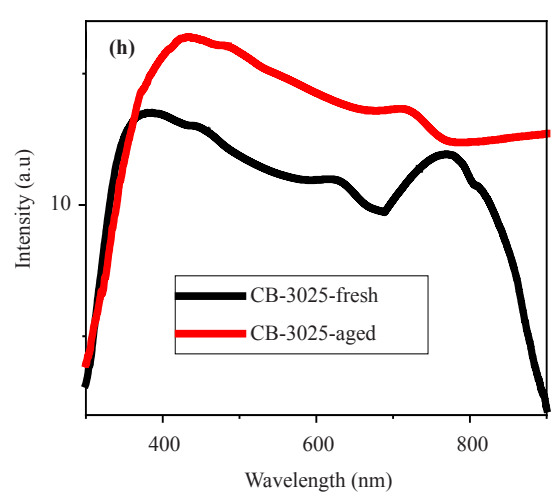
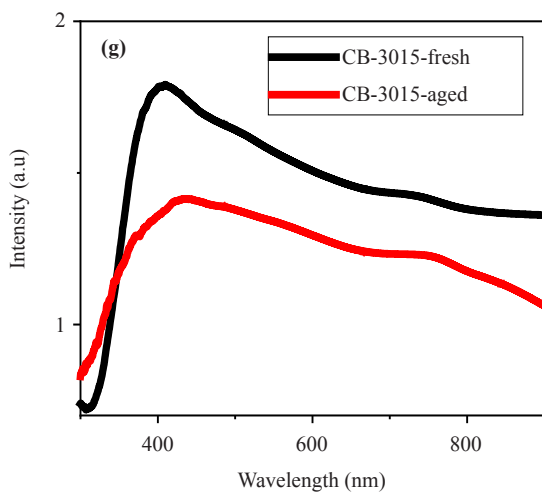
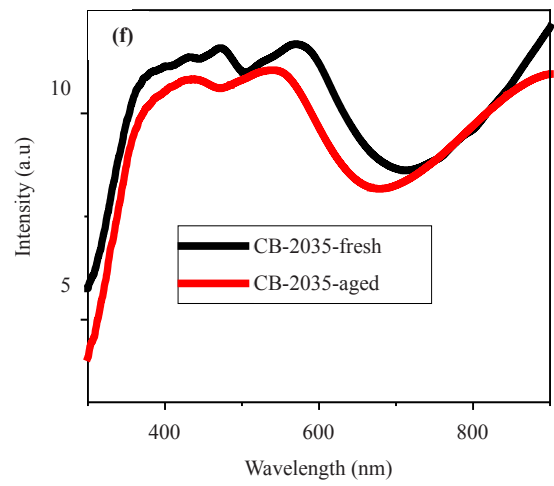
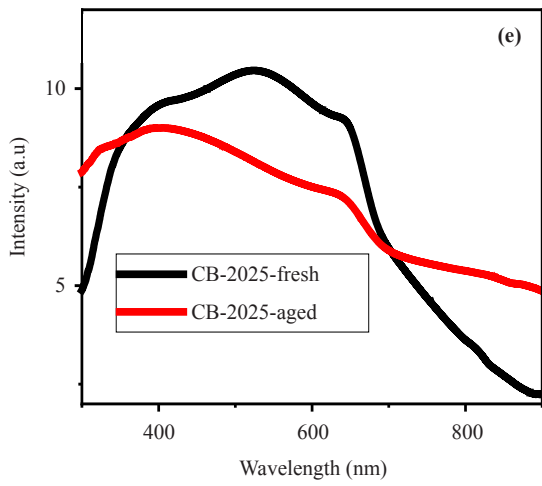
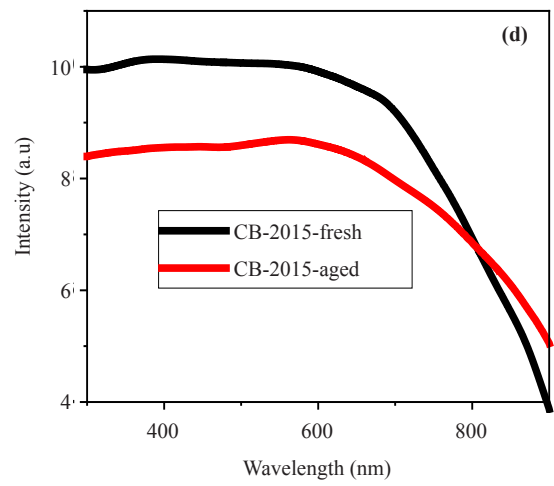
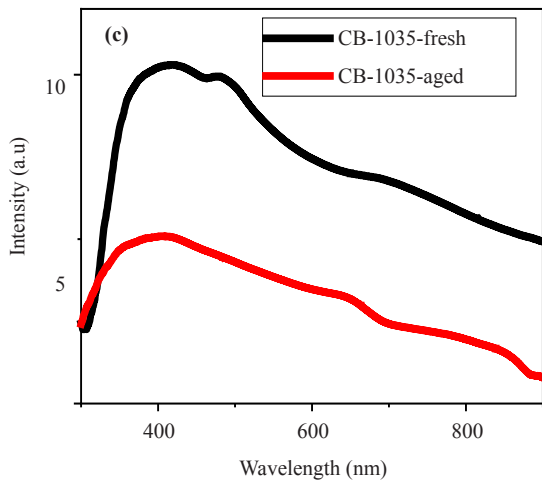
**Table 2.** The calculated band gap and Stokes shift of  $\text{Cs}_x\text{FA}_{1-x}\text{Pb}(\text{I}_{1-y}\text{Br}_y)_3$  perovskite films

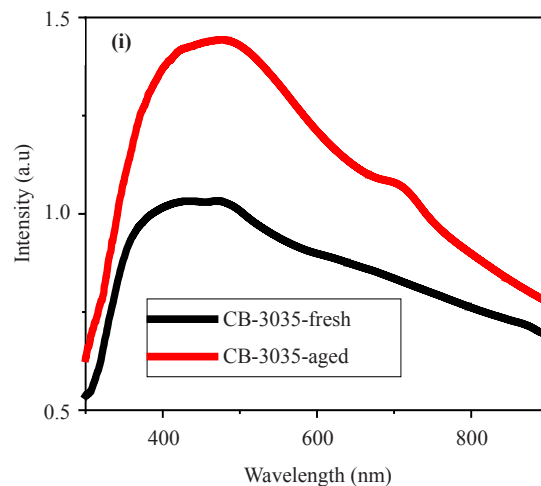
	Absorbance	Photoluminescence	Stokes Shift
	$E_g$ (eV)	$E_g$ (eV)	(eV)
CB-1015	1.62	1.56	0.06
CB-1025	1.68	1.47	0.21
CB-1035	1.7	1.62	0.08
CB-2015	1.62	1.61	0.01
CB-2025	1.68	1.59	0.09
CB-2035	1.7	1.61	0.09
CB-3015	1.62	1.60	0.02
CB-3025	1.72	1.60	0.12
CB-3035	1.75	1.62	0.13

Figure 7b displays the photoluminescence pattern of the different  $\text{Cs}_x\text{FA}_{1-x}\text{Pb}(\text{I}_{1-y}\text{Br}_y)_3$  ( $x = 0.1, 0.2$  and  $0.3$  and  $y = 0.15, 0.25$  and  $0.35$ ) films. The PL emission energy edge did not vary in the same trend as the content of the bromide halide in the overall compound. We observed the lowest energy (highest wavelength, 844 nm) with the CB-1025 and the highest energy (lowest wavelength, 764 nm) with the CB-1035. In terms of intensity and just like with the absorbance, the CB-1015 came far ahead compared to the others.

Three weeks after the first optical properties measurement, we did perform a new evaluation and compared it with the initial one as displayed in figure 8. The red lines are the curves of the films after the three weeks while the black are the original ones at fresh.







**Figure 8.** UV-vis Absorbance spectra of the fresh and 3 weeks old  $\text{Cs}_x\text{FA}_{1-x}\text{Pb}(\text{I}_{1-y}\text{Br}_y)_3$  ( $x = 0.1, 0.2, 0.3$  and  $y = 0.15, 0.25, 0.35$ ) perovskite films

The optical properties checking after three weeks revealed a very little reduction in absorbance for 5 films out of the 9. These 5 are CB-1015, CB-1025, CB-2035, CB-3025 and CB-3035 respectively shown on the Figure 8a-Figure 8g. The last 2 even displayed an increased absorbance. This particular point is an opened door for further investigation to figure out the reason if it is related to a slight change of setting in the measurement method between the first and the second measurement or another thing.

In all cases, we noted the higher stability of the 5 films and much more for the last two and this was perfectly in line with the XRD patterns.

### 3.3 Morphology assessment

The assessment of the morphology of the perovskite thin films was conducted using a Field Emission Scanning Electron Microscope (FESEM). The used device is an ULTRA 55 make of ZEISS, with a setting of detectors composed of SE2 secondary electron detector, secondary electron detector in len, the detector of backscattered electrons AsB, backscattered electron detector in lens EsB and X-ray dispersive energy detector (EDS) of GEMINI technology [37].

The FESEM works with a field emission cannon, a source of electrons, that provides very focused electron beams, which excite and extract secondary electrons from the assessed sample. These secondary electrons are captured by detectors and this generates varieties of signals that provide information on the surface morphology and composition of the material.

The FESEM images, as illustrated in Figure 9, exhibited different morphologies for the  $\text{Cs}_x\text{FA}_{1-x}\text{Pb}(\text{I}_{1-y}\text{Br}_y)_3$  ( $x = 0.1, 0.2, 0.3$  and  $y = 0.15, 0.25, 0.35$ ) samples. More visible on the  $10\mu\text{m}$  scale, the grain size was less for the lower content of bromide in the lattice. The  $1\mu\text{m}$  scale revealed a better crystallinity of the CB-1015, CB-1025, CB-3035 and also the CB-2025. As for the CB-1035 and CB-2015 films, they did not exhibit very regular patterns as a consequence of their lower stability. The crystallinity expresses the degree of long-range structural order in the material. So, the higher the crystallinity, the more atoms or molecules then the crystals and grains will be arranged consistently and repetitively. When the material degrades by lack of stability, this order is partly broken and the grains appear more scattered like for the CB-1035 and CB-2015 samples.

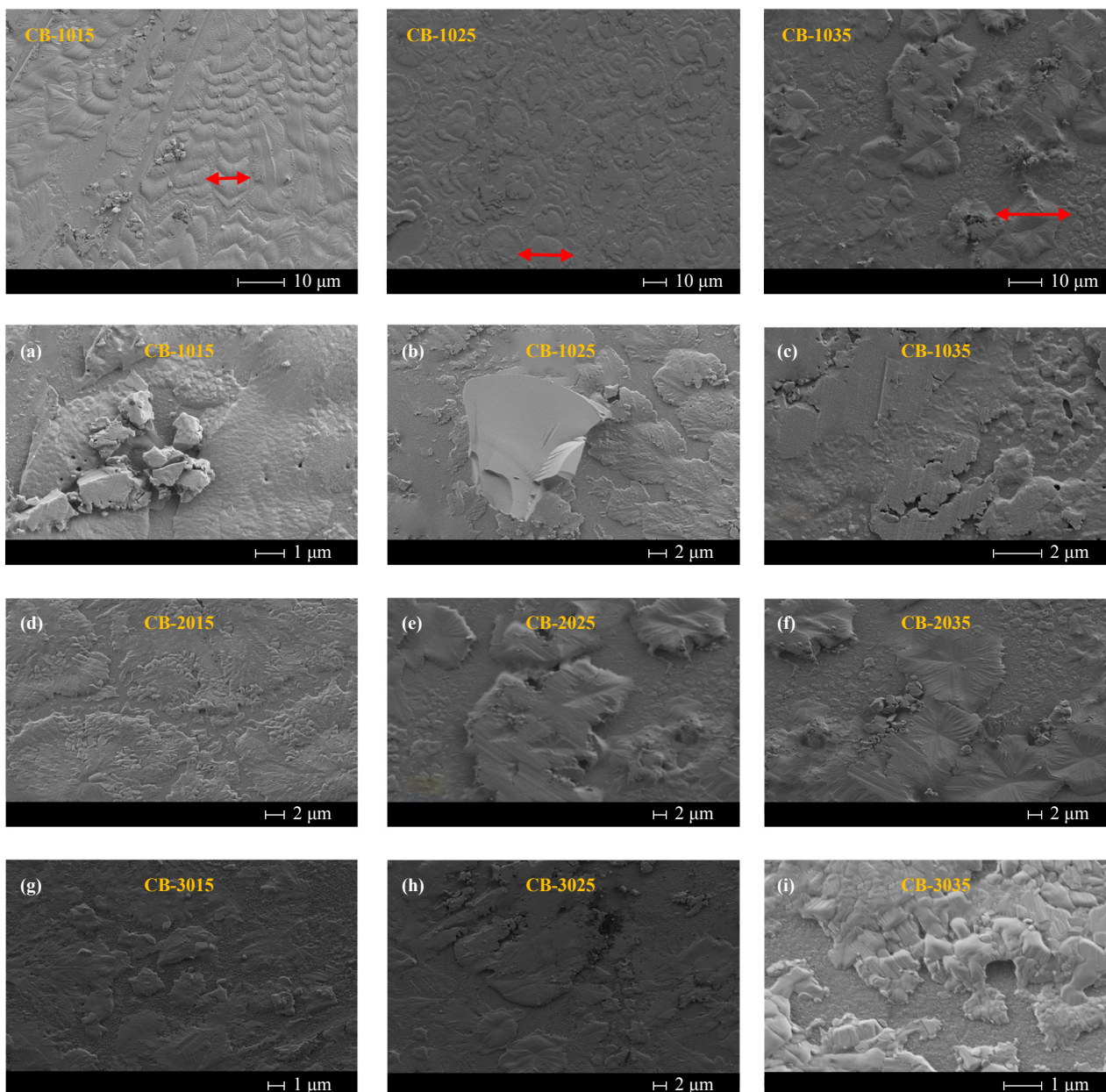


**Figure 9.** FESEM Images of  $\text{Cs}_x\text{FA}_{1-x}\text{Pb}(\text{I}_{1-y}\text{Br}_y)_3$  ( $x = 0.1, 0.2, 0.3$  and  $y = 0.15, 0.25, 0.35$ ) perovskite film

## 4. Conclusions

We successfully explored the way to boost, at room temperature, the stability and performance of the lead halide perovskite by double mixture in the A-cation and X-halide captions. In the course of the investigation, we prepared, at the laboratory ambient conditions, 9 samples of  $\text{Cs}_x\text{FA}_{1-x}\text{Pb}(\text{I}_{1-y}\text{Br}_y)_3$  ( $x = 0.1, 0.2, 0.3$  and  $y = 0.15, 0.25, 0.35$ ) perovskite thin films and characterized their structure by the X-ray diffraction, optical properties by UV-visible spectrometer and morphology by the FESEM technic.

We noted, in contrast to the  $\text{FAPbI}_3$  and  $\text{CsPbI}_3$ , the known most promising non-mixed perovskite materials but which unfortunately quickly shift their structure to non-perovskite phase at room temperature, that the multi-anion-multi-cation halide perovskites exhibited, after three weeks, much better structural stability and kept their perovskite

cubic structure. Besides, we could do a post-annealing of these mixed perovskites at a lower temperature of 120 °C where non-mixed, particularly the CsPbI<sub>3</sub>, require a post-annealing temperature of above 350 °C. The post-annealing at lower temperatures can open doors for deposition of the mixed perovskites on plastic and flexible substrates.

We also noted that, even if it raised a little bit the band gap energy of the perovskite, the content of Br in the material provided increased stability to the overall lattice.

Moreover, and as a confirmation of the structural stability, the mixed perovskites also showed good resistance to the environment moisture with excellent optical properties after three weeks.

Our results are in line with other works on the enhancement of the lead halide perovskite stability and also bring a supplement to them.

The good stability and low-cost processability at room conditions without the high-cost annealing temperature, undisputedly make the simultaneously cation-anion mixed perovskites, good candidates for the escalation and development of solar panels, for the sake of lots of future consumers worldwide.

## Acknowledgements

This work has been funded by Erasmus+ with the Grant KA 107, 2022-2023, the Gobierno de España, Ministerio de Ciencia e Innovación through its program MCIN/AEI/10.13039/501100011033 and also by the Spanish Agencia Estatal de Investigación through the project BESTMAT PID2019-107137RB-C21/AEI/10.13039/501100011033.

## Conflict of interest

The authors declare no competing financial interest.

## References

- [1] Green M, Dunlop E, Hohl-Ebinger J, Yoshita M, Kopidakis N, Hao X. Solar cell efficiency tables (version 57). *Progress in Photovoltaics: Research and Applications*. 2021; 29(1): 3-15.
- [2] Errami M, Garner H. A tale of two citations. *Nature*. 2008; 451(7177): 397-399. Available from: <http://www.nature.com/nature/journal/v451/n7177/full/451397a.html> [Accessed 20th January 2015].
- [3] Touré A, Bouich A, Soucasse BM, Soro D. Investigation of the optoelectronics properties and stability of Formamidinium lead mixed halides perovskite. *Optical Materials*. 2023; 135: 113334. Available from: <https://doi.org/10.1016/j.optmat.2022.113334>.
- [4] Muller M, Marion B, Rodriguez J. Evaluating the IEC 61215 Ed. 3 NMOT procedure against the existing NOCT procedure with PV modules in a side-by-side configuration. *2012 38th IEEE Photovoltaic Specialists Conference*. 2012; 697: 702.
- [5] Ono LK, Juarez-Perez EJ, Qi Y. Progress on perovskite materials and solar cells with mixed cations and halide anions. *ACS Applied Materials & Interfaces*. 2017; 9(36): 30197-30246. Available from: <https://doi.org/10.1021/acsami.7b06001>.
- [6] Hu P, Huang S, Guo M, Li Y, Wei M. Ionic liquid-assisted crystallization and defect passivation for efficient perovskite solar cells with enhanced open-circuit voltage. *ChemSusChem*. 2022; 15(15): e202200819. Available from: <https://doi.org/10.1002/cssc.202200819>.
- [7] Albaladejo-Siguan M, Baird EC, Becker-Koch D, Li Y, Rogach AL, Vaynzof Y. Stability of quantum dot solar cells: A matter of (life) time. *Advanced Energy Materials*. 2021; 11(12): 2003457. Available from: <https://doi.org/10.1002/aenm.202003457>.
- [8] Vega-Fleitas E, Mollar M, Marí B. Synthesis of MAPbBr<sub>3-i</sub>Y<sub>i</sub> (Y = I, Cl and i = 0, 1, 2, 3) thin films perovskite. *Special Issue: E-MRS 2015 Spring Meeting-Symposium D*. 2016; 13(1): 30-34. Available from: <https://doi.org/10.1002/pssc.201510107>.
- [9] Bouich A, Marí-Guaita J, Soucasse BM, Palacios P. Manufacture of high-efficiency and stable lead-free solar cells through antisolvent quenching engineering. *Nanomaterials*. 2022; 12(17): 2901. Available from: <https://doi.org/10.3390/nano12172901>.

- [10] Bouich A, Ullah S, Mari B, Atourki L, Touhami ME. One-step synthesis of  $\text{FA}_{1-x}\text{GA}_x\text{PbI}_3$  perovskites thin film with enhanced stability of alpha ( $\alpha$ ) phase. *Materials Chemistry and Physics*. 2021; 258: 123973. Available from: <https://doi.org/10.1016/j.matchemphys.2020.123973>.
- [11] Barrier J, Beal RE, Gold-Parker A, Vigil JA, Wolf E, Waquier L, et al. Compositional heterogeneity in  $\text{Cs}_y\text{FA}_{1-y}\text{Pb}(\text{Br}_x\text{I}_{1-x})_3$  perovskite films and its impact on phase behavior. *Energy & Environmental Science*. 2021; 4(12): 6394-6405. Available from: <https://doi.org/10.1039/d1ee01184g>.
- [12] Valastro S, Mannino G, Smecca E, Sanzaro S, Deretzis I, La Magna A, et al. Optical behaviour of  $\gamma$ -black  $\text{CsPbI}_3$  phases formed by quenching from 80 °C and 325 °C. *Journal of Physics: Materials*. 2021; 4(3): 034011. Available from: <https://doi.org/10.1088/2515-7639/abfa7a>.
- [13] Doumbia Y, Bouich A, Soro D, Bernabé MS. Improving stability and performance of cesium mixed lead halides for photovoltaic applications. *JOM*. 2023; 75(3): 693-700.
- [14] Beal RE, Hagström NZ, Barrier J, Gold-Parker A, Prasanna R, Bush KA, et al. Structural origins of light-induced phase segregation in organic-inorganic halide perovskite photovoltaic materials. *Soft Matter*. 2020; 2(1): 207-219. Available from: <https://doi.org/10.1016/j.matt.2019.11.001>.
- [15] Coulibaly AB, Oyedele SO, Aka B. Comparative study of lead-free perovskite solar cells using different hole transporter materials. *Modeling and Numerical Simulation of Material Science*. 2019; 9(4): 97-107.
- [16] Derbali S, Nouneh K, Florea M, Neatu F, Neatu S, Leonat LN, et al. Exploring the effect of aliovalent substitution of  $\text{Pb}^{2+}$  by  $\text{Eu}^{3+}$  on structural, morphological and optical properties of  $\text{CH}_3\text{NH}_3\text{PbI}_3$  perovskite films. *Physica Scripta*. 2020; 95(4): 044003. Available from: <https://doi.org/10.1088/1402-4896/ab5baa>.
- [17] Tang G, Wang T, Cao J, Zhao Z, Song J, Liu P, et al. Highly stable and efficient perovskite solar cells passivated by a functional amorphous layer. *Journal of Materials Chemistry A*. 2021; 9(38): 21708-21715.
- [18] Mari-Guaita J, Bouich A, Mari B. Shedding light on phase stability and surface engineering of formamidinium lead iodide ( $\text{FAPbI}_3$ ) thin films for solar cells. *Engineering Proceedings*. 2021; 12(1): 1.
- [19] Dey A, Ye J, De A, Debroye E, Ha SK, Blatt E, et al. State of the art and prospects for halide perovskite nanocrystals. *ACS Nano*. 2021; 15(7): 10775-10981.
- [20] Nonomura R, Oku T, Ono I, Suzuki A, Okita M, Fukunishi S, et al. Effects of cesium/formamidinium co-addition to perovskite solar cells. *Engineering Proceedings*. 2022; 31(1): 32.
- [21] Derbali S, Nouneh K, Florea M, Leonat LN, Stancu V, Tomulescu AG, et al. Potassium-containing triple-cation mixed-halide perovskite materials: Toward efficient and stable solar cells. *Journal of Alloys and Compounds*. 2021; 858: 158335.
- [22] Mundt LE, Zhang F, Palmstrom AF, Xu J, Tirawat R, Kelly LL, et al. Mixing matters: Nanoscale heterogeneity and stability in metal halide perovskite solar cells. *ACS Energy Letters*. 2021; 7(1): 471-480.
- [23] Liu D, Yang C, Bates M, Lunt RR. Room temperature processing of inorganic perovskite films to enable flexible solar cells. *IScience*. 2018; 6: 272-279.
- [24] Mari-Guaita J, Bouich A, Mari B. Shedding light on phase stability and surface engineering of formamidinium lead iodide ( $\text{FAPbI}_3$ ) thin films for solar cells. *Engineering Proceedings*. 2021; 12(1): 1.
- [25] Stewart AW, Bouich A, Soucase BM. Enhancing the stability and crystallinity of  $\text{CsPbIBr}_2$  through antisolvent engineering. *Journal of Materials Science*. 2021; 56: 20071-20086. Available from: <https://doi.org/10.1007/s10853-021-06552-3>.
- [26] Ullah S, Bouich A, Ullah H, Mari B, Mollar M. Enhanced optical and structural properties of V-doped binary  $\text{SnS}_2$  buffer layer. *Solar Energy*. 2020; 204: 654-659.
- [27] Wang Y, Liu X, Zhang T, Wang X, Kan M, Shi J, et al. The role of dimethylammonium iodide in  $\text{CsPbI}_3$  perovskite fabrication: additive or dopant? *Angewandte Chemie*. 2019; 131(46): 16844-16849.
- [28] Koné KE, Bouich A, Mari-Guaita J, Soucase BM, Soro D. Insight into the effect of halogen X in methylammonium lead halide ( $\text{MAPbX}_3$ ) spin-coated on zinc oxide film. *Optical Materials*. 2023; 135: 113238.
- [29] Bouich A, Mari-Guaita J, Sahraoui B, Palacios P, Mari B. Tetrabutylammonium (TBA)-Doped Methylammonium Iodide: High quality and stable Perovskite thin films. *Frontiers in Energy Research*. 2022; 10: 840817.
- [30] Bouich A. *Study and characterization of hybrid perovskites and copper-indium-gallium selenide thin films for tandem solar cells*. Valencia, Spain. Universitat Politècnica de València; 2021.
- [31] Bouich A, Mari-Guaita J, Bouich A, Pradas IG, Mari B. Towards manufacture stable lead perovskite  $\text{APbI}_3$  (A = Cs, MA, FA) based solar cells with low-cost techniques. *Engineering Proceedings*. 2022; 12(1): 81.
- [32] Chfii H, Bouich A, Soucase BM, Abdlefdil M. A new approach for growing high-quality delafossite  $\text{CuCoO}_2$  films by spray pyrolysis through the optimization of the Cu/Co ratio. *Optical Materials*. 2023; 135: 113229.
- [33] Yin J, Li H, Cortecchia D, Soci C, Bredas JL. Excitonic and polaronic properties of 2D hybrid organic-inorganic perovskites. *ACS Energy Letters*. 2017; 2(2): 417-423.

- [34] Bush KA, Frohna K, Prasanna R, Beal RE, Leijtens T, Swifter SA, et al. Compositional engineering for efficient wide band gap perovskites with improved stability to photoinduced phase segregation. *ACS Energy Letters*. 2018; 3(2): 428-435.
- [35] Jubu PR, Yam FK, Igba VM, Beh KP. Tauc-plot scale and extrapolation effect on bandgap estimation from UV-vis-NIR data-a case study of  $\beta$ -Ga<sub>2</sub>O<sub>3</sub>. *Journal of Solid State Chemistry*. 2020; 290: 121576.
- [36] Tian Y, Scheblykin IG. Artifacts in absorption measurements of organometal halide perovskite materials: What are the real spectra? *The Journal of Physical Chemistry Letters*. 2015; 6(17): 3466-3470.
- [37] Vega Fleitas E. *Study and characterization of hybrid organic-inorganic perovskites for solar cells applications*. Valencia, Spain. Universitat Politècnica de València; 2018.